The potential of small unmanned aircraft systems and structure-from-motion for topographic surveys: A test of emerging integrated approaches at Cwm Idwal, North Wales

T.N.Tonkin[a1], N.G.Midgley[a] , D.J.Graham[b], J.C.Labadz[a]

[a]School of Animal, Rural and Environmental Sciences, Nottingham Trent University, Brackenhurst Campus, Southwell, Nottinghamshire NG25 0QF, UK

[b]Polar and Alpine Research Centre, Department of Geography, Loughborough University, Leicestershire LE11 3TU, UK

[1]Corresponding author. Tel.: + 44 115 848 5257. toby.tonkin@ntu.ac.uk

Abstract

Novel topographic survey methods that integrate both structure-from-motion (SfM) photogrammetry and small unmanned aircraft systems (sUAS) are a rapidly evolving investigative technique. Due to the diverse range of survey configurations available and the infancy of these new methods, further research is required. Here, the accuracy, precision and potential applications of this approach are investigated. A total of 543 images of the Cwm Idwal moraine-mound complex were captured from a light (< 5 kg) semi-autonomous multi-rotor unmanned aircraft system using a consumer-grade 18 MP compact digital camera. The images were used to produce a

DSM (digital surface model) of the moraines. The DSM is in good agreement with 7761 total station survey points providing a total vertical RMSE value of 0.517 m and vertical RMSE values as low as 0.200 m for less densely vegetated areas of the DSM. High-precision topographic data can be acquired rapidly using this technique with the resulting DSMs and orthorectified aerial imagery at sub-decimetre resolutions. Positional errors on the total station dataset, vegetation and steep terrain are identified as the causes of vertical disagreement. Whilst this aerial survey approach is advocated for use in a range of geomorphological settings, care must be taken to ensure that adequate ground control is applied to give a high degree of accuracy.

Highlights

- An integrated sUAS and SfM approach is used to generate high-resolution topographic data.
- SfM data compared with a total station ground survey.
- Positional errors on the total station dataset, vegetation and steep terrain are identified as causes of vertical difference between the two datasets.
- The integration of a combined sUAS and SfM approach is discussed.

Keywords

Small unmanned aircraft system, Structure from motion, Digital surface model, Digital elevation model, Topographic surveying

1 Introduction

The use of small unmanned aircraft systems (sUAS) and structure-from-motion (SfM) digital photogrammetry presents a new methodological frontier for topographic data acquisition and is of interest to scientists researching in a range of geomorphological environments (Westoby et al., 2012; Carrivick et al., 2013; Hugenholtz et al., 2013; Tarolli, 2014). Traditionally low-level aerial photography has been acquired using a variety of unmanned platforms including small lighter-than-air blimps, kites, and model fixed-wing and single rotor aircraft (e.g. Wester-Ebbinghaus, 1980; Rango et al., 2009; Smith et al., 2009; Hugenholtz et al., 2013). More recently lightweight (< 5 kg), relatively low-cost multi-rotor aerial platforms have been used to capture low-level imagery (Harwin and Lucieer, 2012; Niethammer et al., 2012; Rosnell and Honkavaara, 2012; Mancini et al., 2013; Lucieer et al., 2014). These sUAS can be programmed to fly semi-autonomously at fixed altitudes along flight lines, ensuring optimal image overlap for digital photogrammetry. A key strength of the integrated sUAS–SfM approach is the degree of automation involved. Previously, a high degree of user experience was a prerequisite for both the operation of aerial platforms and the application of photogrammetric methods to extract meaningful topographic data from aerial imagery (Aber et al., 2010). The premise of SfM as a digital photogrammetric technique is that three-dimensional coordinates can be extracted from sufficiently overlapping photography without the need for camera spatial information (Snavely et al., 2008; Westoby et al., 2012). The integration of SfM with sUAS camera platforms offers a rapid and increasingly cost effective option for geomorphologists to produce digital surface models (DSMs), with resolution and data quality proposed to be on-par with, or better than LiDAR (Carrivick et al., 2013; Fonstad et al., 2013). SfM based topographic surveys have

recently been used for a variety of geoscientific applications including quantifying rates of landslide displacement (Lucieer et al., 2013), mapping vegetation spectral dynamics (Dandois and Ellis, 2013), producing DEMs (digital elevation models) of agricultural watersheds (Ouédraogo et al., 2014), quantifying coastal erosion rates (James and Robson, 2012), and measuring rates of glacier motion and thinning (Whitehead et al., 2013). The potential of SfM to aid geomorphological mapping, derive measurements of landforms (morphometry) and quantify geomorphological change is evident. Numerous software packages for SfM are now available and include cloud-based processing, which has the additional benefit of not requiring a high-specification consumer computer capable of handling the image processing.

Whilst a range of recent studies have sought to quantify data quality and associated error of SfM techniques (Harwin and Lucieer, 2012; Turner et al., 2012; Westoby et al., 2012; Dandois and Ellis, 2013; Fonstad et al., 2013; Hugenholtz et al., 2013; Ouédraogo et al., 2014), further research is beneficial due to the diverse nature of the aerial platforms and consumer-grade digital cameras available for the production of topographic data using this methodology. Existing reports on the effectiveness of integrated multi-rotor based sUAS–SfM approaches describe surveys conducted from relatively low altitudes (< 50 m). The aims of this research are to: (1) provide a systematic account of the data acquisition process associated with this new integrated technique; (2) compare vertical spot heights obtained from the sUAS–SfM survey to those obtained from a total station ground survey; (3) highlight important considerations for researchers seeking to use sUAS and SfM approaches to acquire data for topographic investigations; and (4) provide a baseline for the potential

spatial resolutions when using a consumer-grade 18 MP compact digital camera at a target flight altitude of 100 m.

2 Study area

The test was undertaken at Cwm Idwal, north Wales (53° 6′50.89″N; 4° 1′38.38″W; Fig. 1) (Appendix A), a large cirque that was last occupied by a glacier during the Younger Dryas Stadial (c.12.9-11.7 ka BP; Bendle and Glasser, 2012). The study area is located on the cirque floor and covers an altitudinal range of ~ 370 to ~ 410 m (above ordnance datum). The geomorphology of the site is characterised by a moraine-mound complex ('hummocky moraine') located on both the east and west of Llyn [lake] Idwal (Fig. 1c). These moraines have been the subject of numerous investigations (e.g. Darwin, 1842; Escritt, 1971; Gray, 1982; Addison, 1988; Graham and Midgley, 2000; Bendle and Glasser, 2012) due to their importance for understanding the significance of Younger Dryas glaciers in the British Uplands. The majority of the moraines are 8 to 80 m in length, with the exception being a set of discontinuous stream-breached ridges totalling ~450 m in length which are stacked against the western cirque wall. In places the morphology of the moraines are influenced by glacially abraded bedrock. The prominence of some landforms is also disguised by a peat infill. The southern section of the survey area is characterised by a relatively flat lake infill and steep glacially abraded bedrock slopes. Vegetation on the eastern side of the Cwm is typically restricted to short swards of grass, whereas livestock grazing exclosures erected in the 1950s and 1960s on the western side of Llyn Idwal have promoted the growth of vegetation including a thick cover of common heather (Calluna vulgaris), western gorse (Ulex gallii), and the occasional

rowan (Sorbus aucuparia) and silver birch (Betula pendala) (Rhind and Jones, 2003). A large part of the moraine-mound complex and surrounding area were surveyed with a total station by Graham and Midgley (2000). A similar area was surveyed by a sUAS to allow a direct comparison between total station based data acquisition, and the sUAS–SfM method used for this study.

3 Methods and materials

3.1 Image Image and data acquisition

Aerial imagery was acquired using a Canon EOS-M 18 MP camera suspended from a DJI S800 Hexacopter (Fig. 2). A Photohigher AV130 servo driven gimbal maintained the camera angle close to the nadir. The hexacopter was equipped with a Wookong-M GPS assisted flight controller which allowed for semi-autonomous surveys. Survey flight-lines were pre-programmed via the DJI Ground-Station software package. For all surveys the sUAS was set to a target altitude of 100 m above ground level (AGL) and horizontal ground speed of 2.5 ms^{-1}. The target altitude is calculated in the DJI Ground-Station software using elevation data derived from Google Earth. Parallel flights lines were programmed to have an image sidelap of 80%, whilst taking into account the camera sensor size (22.3 × 14.9 mm) and focal length (22 mm). The intervalometer function of the Magic Lantern third-party camera firmware was set to acquire imagery every 2 s along parallel flight lines. Actual image acquisition was every ~ 4 s, resulting in image capture approximately every 10 m along flight lines. Although image capture can be triggered using the DJI flight controller, an intervalometer was used for its improved reliability and potential to capture excess imagery along flight lines. This allowed for blurred or poor quality

142 imagery to be removed whilst ensuring that an image onlap in excess of 80% was
143 maintained. The camera was set to shutter-priority mode and used a 1/1000 s
144 shutter speed. To provide the required image coverage the survey area had to be
145 split between four flights. The sUAS had a flight-time of ~ 14 min whilst carrying its
146 payload (using an 11 Ah, 22.2 V, 6 cell lithium polymer battery). A generous
147 overhead (~ 2 min) was left in order to safely land the sUAS. In the UK unaided
148 visual line of sight (VLOS) has to be maintained whilst operating sUAS (CAA, 2012).
149 Therefore the ground equipment and launch position were moved between flights to
150 allow the sUAS to be easily observed, and manually controlled if necessary.

151

152 The total station dataset was acquired over multiple survey sessions in 1997 and
153 1998 using a Leica TC600 (Graham and Midgley, 2000). An assessment of error for
154 this data set is unavailable. However, measurement accuracies (expressed as
155 standard deviation) for the TC600 are defined by Leica (1997), with distance
156 measurements accurate to 2 mm ± 2 ppm and angle (horizontal and vertical)
157 measurements to 1.5 mgon. As the original total station dataset was collected for
158 the purpose of characterising the overall shape of the moraine-mound complex,
159 individual points were collected rapidly. Points recorded whilst the prism pole was
160 not perfectly vertical have the potential to result in misregistration between the two
161 datasets. The extent of the resulting error will be exacerbated by slope steepness
162 and the height of the reflector on the detail pole. The SfM dataset was tied into the
163 same arbitrary co-ordinate system and datum through the use of two brass pin
164 benchmarks located on exposed bedrock on the east and west of Llyn Idwal. Point
165 densities for the validation points reach as high as 20 per 100 m2 over the moraine-
166 mound complex (Graham and Midgley, 2000). For the sUAS survey, 19 SfM ground-

control points (GCPs) were distributed across the survey area (Fig. 3a). White laminated A3 size targets (297 × 420 cm) were used as GCPs and were found to be adequately visible on the aerial imagery. These GCPs were surveyed with a Leica TC407 total station to a precision of ≤ 1 mm and estimated accuracy of < 3 cm.

3.2 Image processing and analysis

From the original set of 824 images, 543 images were selected for model reconstruction using the Agisoft Photoscan 1.0.0 (build 1795) software package. Images were visually assessed for quality and blurry images were removed prior to processing. Image processing followed the recommended procedure outlined by Agisoft (2013). Image processing was conducted on a HP Z820 workstation equipped with dual Intel Xeon E5-2690 processors, 128 GB RAM, and nVidia 680 graphics card. As GPS information for camera positions were not collected, images were aligned using the 'Generic Pair Preselection' parameter. This parameter detects matching features between images at a lower accuracy first, to reduce overall processing time (Agisoft, 2013). Photoscan provides nominal parameters for setting the target accuracy to which the images are aligned. Here the 'high' setting was used to obtain the best possible image alignment accuracy. Nineteen GCPs were then identified on imagery within the software a total of 674 times, with the XYZ coordinates input for each point. The sparse point cloud was optimised using a marker accuracy of 0.001 m and focal parameters (F_y and F_x) defined in the image headers. Camera radial and tangential distortion coefficients (K_1, K_2, K_3, P_1 and P_2) were automatically estimated by Photoscan. A dense point cloud was then produced using the 'medium' quality setting. Again, this is a nominal setting that relates to the

191 geometric accuracy of the target dense point cloud produced within Photoscan.
192 Aggressive depth filtering was used to remove outliers from the dense point cloud
193 (Agisoft, 2013). The dense point cloud and polygonal mesh was generated using a
194 target point count of 3×10^5. An additional sparse point cloud and a DSM were
195 produced for comparative purposes. An orthorectified aerial image was produced
196 using the 'orthophoto' and 'mosaic' parameters with colour correction enabled.
197 Where image overlap occurs, the 'mosaic' parameter ensures that images with pixels
198 closest to the image centre are used preferentially for orthophoto generation (Agisoft,
199 2013).

200

201 Data handling and the analysis of geographic data were conducted using
202 QuantumGIS 2.0 and ArcGIS 10.1. SfM height (SfMz) was subtracted from ground
203 height (GSz) for 7761 independently surveyed data validation spot heights derived
204 by total station survey (Fig. 3a) providing a vertical difference. The vertical difference
205 was converted into a raster surface with a 2.1 m cell size using an ordinary kriging
206 function in ArcGIS 10.1. This allowed the vertical difference to be visualised. RMSE
207 (root mean square error) and MD (mean difference) were calculated for the vertical
208 difference (SfMz−GSz). Two zones of contrasting vegetation cover (Z1 and Z2; Fig.
209 3a) were mapped from orthorectified aerial imagery, and used to quantify vertical
210 difference associated with contrasting vegetation types. Z1 is characterised by a
211 continuous ground cover of heather, gorse, and occasional shrub and is located on
212 the western side of Llyn Idwal. Z2 consists of grassland and exposed bedrock, and is
213 also located on the western side of Llyn Idwal.

214

4 Results

The dense point cloud was composed of 31,474,859 unique points. With the exception of the extremities of the model, the effective overlap was > 9 images per point. 'Noisy' anomalies are present where the surface of reflective water-bodies are reconstructed. The orthorectified images had a 0.022 m per pixel resolution, and the DSM as seen in Fig. 3b had a 0.088 m per pixel resolution. These resolutions were achieved from an average flight altitude of 117.282 m AGL as reconstructed from the imagery. Discrepancy between the target flight attitude and actual flight attitude is likely to be caused by the use of low resolution Google Earth elevation data for flight planning, and error associated with the use of barometric pressure sensors for determining relative height (see DJI, 2013). Photoscan reported a total RMSE value of 0.033 m, calculated from the 19 SfM GCPs. The total x and y RMSE values reported by Photoscan were 0.019 and 0.020 m respectively. The total vertical RMSE value was 0.018 m.

Spot heights (n = 7761) from the ground survey (GSz) and DSM (SfMz) are in broad agreement, although the vertical difference is a higher than that reported by the 19 SfM GCPs used during the image processing stage. The vertical difference is visualised in Fig. 3c. The dense point cloud provides a vertical RMSE value of 0.517 m (Table 1). The differences for the DSM are offset from zero, with a mean difference of 0.454 m. The majority of the height values on the DSM were within the ± 1 m range (99.8%). However, only 55.4% of the SfM DSM values were within ± 0.5 m of the ground survey data. Isolated spot heights were found to be as much as − 0.705 m under the actual ground survey (GSz) and as much as 4.347 m over.

When vertical RMSE is calculated separately, RMSE for the east (less densely vegetated) is significantly lower (RMSE = 0.200; n = 1988), than the west (RMSE = 0.588; n = 5773) with 98.8% of height values for the east falling within the ± 0.5 m range (Fig. 4).

Two contrasting vegetation zones (Z1 and Z2 in Fig. 3a) were investigated. Z1 had an RMSE value of 0.789 m (n = 244). In contrast, Z2 produced a lower RMSE value of 0.362 m (n = 205). The calculated RMSE values for slopes gentler than 20° and those steeper than or equal to 20° were examined for both patches. The values are 0.031 and 0.030 m higher for slopes steeper than 20° regardless of the vegetation type. Where RMSE was calculated for separate 10° bins for the entire dataset (7761 observations), excluding the 60–70° bin, the reported RMSE value increases on progressively steeper slopes (0.444 to 0.838; Table 2). The 80–90° bin comprised one observation, which shows a high vertical difference (2.222 m).

An additional analysis of the DSM derived from the sparse point cloud (2,058,037 points) was conducted. The sparse point cloud produced a coarser resolution DSM at 0.258 m per pixel. Unlike the dense point cloud, the sparse point cloud did not produce ‘noisy’ anomalies related to reflective water-bodies. Points from the SfM DSM and the ground survey data were also in broad agreement with 98.9% of the data within the ± 1 m range, and 58.5% of the data in the ± 0.5 m range. The total vertical RMSE value was 0.505 m. The sparse point cloud derived DSM produced a wider range of outlying values, with minimum and maximum anomalies of − 3.416 and 3.782 m.

5 Discussion

5.1 Causes of vertical disagreement

Causes of poor surface representation and vertical disagreement between the two data sets have been investigated and include: (1) vegetation; (2) slope angle; and (3) unintentional random error related to the acquisition of the original total station dataset. Vegetation is a known cause of poor surface representation in DEMs derived from both photogrammetry (Lane, 2000; Marzolff and Poesen, 2009), and airborne LiDAR (Lui, 2008; Spaete et al., 2011; Hladik and Alber, 2012). A visual assessment of high vertical difference against the orthorectified imagery shows that error is particularly pronounced around trees, and in areas vegetated with heather (Fig. 5a). Dense vegetation types obstruct line-of-sight of actual ground level, thus generate a vertical difference between the two datasets (Table 1). This difference generated by vegetation is also apparent when the east (sparsely vegetated) and west (densely vegetated) are visualised together (Fig. 3c) or where RMSE is calculated for the two zones of contrasting vegetation (Z1 and Z2). For the examples of Z1 (heather and other shrubs) and Z2 (grasses and exposed bedrock), the presence of a thick covering of vegetation produces an additional 0.434 m RMSE value (Table 1). Whilst the total station data provides information that can be used to produce a bare earth DEM of the moraines, the data presented from SfM photogrammetry accounts for the surface plus vegetation, and therefore represents a DSM. Fig. 5a exemplifies this error, showing how a ground survey point located under a silver birch generates a vertical difference between the two datasets. Similarly, in other areas of the Cwm Idwal DSM, this problem arises due to tilted bedrock rafts with near vertical and in places overhanging sides (Fig. 5b), generating the outlying vertical difference of 4.347 m. As DSMs are essentially 2.5 dimensional

representations of the earth's surface and associated surface features, true 3 dimensional representation of overhanging surfaces is not possible (Bernhardsen, 2002). If the same SfM approach was applied to un-vegetated terrain (e.g. braided channels in Javernick et al., 2014), a significantly lower degree of vertical difference would be expected.

Further vertical differences between the two topographic datasets is also likely to be the result of unintentional random errors in the ground survey dataset caused by the reflector detail pole not being held perfectly level during point acquisition. The vertical difference caused by this operational error appears to be exacerbated on steep slopes (Table 2). For example, on a perfectly horizontal surface, if the reflector (with the detail pole set to the minimum high of 1.3 m) was inclined at 10° from vertical opposed to being perfectly vertical, the calculated positional and vertical errors would be 0.226 and 0.020 m respectively. However, if the detail pole was inclined at 10° from vertical on a slope of 30°, the expected vertical error would reach the decimetre range. As 16.3% of the 7761 observations were made on slopes > 30°, additional errors should be expected. An example where positional misregistration between the two datasets has occurred is presented in Fig. 5c. Here points taken in the vicinity of a steep-sided tilted bedrock raft with near vertical slopes have resulted in vertical disagreement exceeding 1 m. In this circumstance, sub-decimetre positional errors on the ground survey data or poorly resolved features on the SfM DSM promote a high degree of localised vertical disagreement between the two datasets.

311 *5.2 Benefits and practical considerations*

312 The sUAS-SfM technique is in many ways superior to a conventional total station
313 ground survey and performed comparably to a range of recent SfM data validation
314 studies (Table 3). Whilst the total station topographic survey reported by Graham
315 and Midgley (2000) took approximately 15 field-days, this aerial survey was
316 completed in 3 days and also provided high-resolution aerial imagery. The
317 standalone sUAS survey could have feasibly been completed in one day, however
318 this survey needed to be tied into the arbitrary coordinate system and datum used by
319 Graham and Midgley (2000). Operation of the sUAS is unfortunately restricted to dry
320 conditions, with relatively low wind speeds (< 8 ms^{-1}). Despite specific weather
321 requirements, multi-rotor based systems appear to be well-suited to mountain
322 settings. They can be deployed where there is limited space for take-off and landing,
323 and offer a high-degree of control, which is beneficial when surveying in close
324 proximity to steep slopes. Regardless of the sUAS platform used for image
325 acquisition, the technique lends itself to surveying unstable or inaccessible terrain
326 where traditional survey methods would be unfeasible or unsafe.

327

328 UAS based image acquisition has clear benefits over existing full-scale airborne
329 image acquisition as the low survey altitude circumvents much of the weather
330 dependency (particularly cloud coverage) that affect full-scale airborne surveys
331 (Baltsavias, 1999). UAS also have the additional co-benefits of being less costly to
332 deploy in comparison to full scale airborne surveys and have the ability to produce
333 data products that are more scale appropriate for micro topographic investigations
334 than those provided by airborne LiDAR (Laliberte and Rango, 2009; Anderson and

335 Gaston, 2013). However, application of the SfM technique may be limited in some
336 geomorphological environments due to the presence of texturally ‘smooth’ or
337 reflective surfaces (e.g. snow cover or sand) which prohibit the extraction of
338 meaningful topographic data (Fonstad et al., 2013). Further work to investigate the
339 performance of automated image alignment over more texturally homogenous
340 surfaces may be beneficial where GPS information for camera positions are not
341 available. Care must be taken when acquiring coordinates for the GCPs used during
342 the image processing stage, due to the potential for erroneous readings to propagate
343 through the various derivative data products. Providing that the GCPs are accurately
344 surveyed, the automated nature of the approach is beneficial as it reduces the
345 potential for unintentional random error (e.g. as found to occur in the total station
346 dataset).

347

348 Although the production of a DSM from a dense point cloud produced a sub-
349 decimetre DSM, a coarser DSM (0.258 m per pixel) can be reconstructed from a
350 sparse point cloud of 2 million points with comparable error to that derived from a
351 dense point cloud of 30 million points. Where computational resources for both
352 image processing and data handling are limited or where data are not required at
353 sub decimetre resolution, producing DSMs from lower point densities maybe
354 desirable. The DSM presented here required ~ 7 h to point match and align the 543
355 images. An additional 43 min of processing time was needed to derive the dense
356 point cloud. Research to investigate the influence of point cloud density and the
357 resulting DSM error merits further investigation, although all DSMs should be
358 regarded as an abstraction, with some associated uncertainty (Fisher and Tate,
359 2006; Wechsler, 2007)

5.3 sUAS–SfM as a tool for geomorphological mapping and monitoring morphometric change

The sUAS–SfM based approach appears to be a useful research tool that aids the production of accurate geomorphological maps. A variety of data sources can be used to compile geomorphological maps (Oguchi et al., 2011), with remotely sensed data often requiring ground-truthing to ensure that landforms are accurately recognised within a study area (Hubbard and Glasser, 2005; Knight et al., 2011). From this perspective the recent availability of high-resolution airborne LiDAR datasets are seen to be beneficial for the production of more accurate geomorphological maps (Jones et al., 2007; Bishop et al., 2012), yet the limited coverage of LiDAR surveys mean researchers do not always have access to high-resolution data. In such cases the sUAS–SfM approach could be utilised by researchers who wish to produce their own ultra-high-resolution DSMs and orthophotos to aid field-mapping campaigns. Researchers should determine whether the spatial coverage offered by sUAS is useful for their investigation. Here, a localised area of 0.211 km^2 was surveyed over four separate flights. This is unlikely to be sufficient for all geoscientific applications, however as sUAS technology improves, greater survey coverage per flight may be permitted.

A further application of sUAS–SfM based surveys is morphometric change detection due to how readily the technique can be deployed for use. Quantification of geomorphological change through the comparison of multi-temporal DEMs is a well-established practice applied to a range of geomorphological settings (coastal, glacial, hillslope, fluvial, etc.; e.g. Pyle et al., 1997; Schiefer and Gilbert, 2007; Dewitte et al.,

2008; Marzolff and Poesen, 2009; Mitasova et al., 2009; Hugenholtz, 2010; Irvine-Fynn et al., 2011; Carrivick et al., 2012). In some cases quantifying morphometric change can be problematic where the rate of change is below or close to the achievable accuracy of a given topographic survey technique (Williams, 2012). SfM integrated with sUAS based image acquisition has recently been used for change detection. For example, Whitehead et al. (2013) successfully completed repeat SfM surveys to report on the thinning and motion of Fountain Glacier (Alaska) over a one year period, with the first survey utilising a fixed wing UAS for image acquisition. Lucieer et al. (2013) also used the sUAS–SfM approach, comparing multi-temporal, multi-rotor derived aerial images to monitor landslide displacements at sub-decimetre accuracies. The now widespread availability of aerial platforms and SfM packages adds the range of mapping and survey techniques available to geomorphologists. The technique is a logical choice due to the achievable survey accuracies and potential to monitor geomorphological change at smaller spatial scales remotely.

6 Conclusions

The integrated use of sUAS and SfM technologies for the acquisition of sub-decimetre resolution DSMs has been investigated. The technique is shown to be superior to conventional total station survey in terms of resolution, time required for data acquisition, and has the additional benefit of providing ultra-high-resolution orthorectified aerial imagery. DSM spatial resolutions of 0.088 m were achieved from an approximate flight altitude of 117 m AGL whilst using a consumer-grade 18 MP digital camera. Unintentional random error on the total station dataset, vegetation

and steep terrain are shown to promote vertical disagreement between the two datasets. Where vegetation is sparse, a vertical difference of 0.200 m RMSE was achieved. Overall, the technique is shown to provide exceptionally high-resolution topographic datasets and aerial imagery. The repeatability of the technique where surveys can be benchmarked or georeferenced using dGPS could offer not only unprecedented spatial resolutions, but also high temporal resolution for monitoring on-going geomorphological processes in a range of environments.

Acknowledgements

The aerial survey component of the research was undertaken whilst TNT was funded by a Nottingham Trent University VC bursary. Nottingham Trent University also provided NGM with funding for the purchase of equipment. The total station survey component of the research was undertaken whilst NGM was in receipt of a studentship at Liverpool John Moores University and DJG was in receipt of a studentship at the University of Wales, Aberystwyth. Permission to work in Cwm Idwal was granted by H. Roberts (Countryside Council for Wales) in 1997 and G. Roberts (Cwm Idwal Partnership Office) in 2013. TNT thanks Tom Biddulph and Rob Davis for their assistance in the field. This manuscript benefitted from comments provided by three anonymous reviewers and Prof. T. Oguchi.

427 **References**

428 Anderson, K and Gaston, K.J. 2013. Lightweight unmanned aerial vehicles will
429 revolutionize spatial ecology. *Frontiers in Ecology and the Environment*, **11** (3), 138-
430 146. http://dx.doi.org/10.1890/120150

431

432 Aber, J.S., Marzolff, I., Ries, J.B. 2010. Small-format aerial photography: Principles,
433 techniques and geoscience applications. Elsevier, Amsterdam, pp 268.

434

435 Addison, K. 1988. The Ice Age in Cwm Idwal, 2nd edition. Shropshire; pp 16.

436

437 Agisoft. 2013. Agisoft PhotoScan User Manual: Professional Edition. Retrieved
438 23/10/2013: http://www.agisoft.ru/products/photoscan/professional/

439

440 Baltsavias, E.P. 1999. A comparison between photogrammetry and laser scanning.
441 *ISPRS Journal of Photogrammetry and Remote Sensing*. **54** (2–3), 83-94.
442 http://dx.doi.org/10.1016/S0924-2716(99)00014-3

443

444 Bendle, J.M and Glasser, N.F. 2012. Palaeoclimatic reconstruction from Lateglacial
445 (Younger Dryas Chronozone) cirque glaciers in Snowdonia, North Wales.
446 *Proceedings of the Geologists' Association*, **123**, 130-145.
447 http://dx.doi.org/10.1016/j.pgeola.2011.09.006

448

449 Bernhardsen, T. 2002. *Geographic Information Systems: An Introduction*, John Wiley
450 & Sons: New York, pp 448.
451
452 Bishop, M.P., James, L.A., Shroder Jr, J.F. and Walsh, S.J. 2012. Geospatial
453 technologies and digital geomorphological mapping: Concepts, issues and research.
454 *Geomorphology*. **137**(1), 5-26. http://dx.doi.org/10.1016/j.geomorph.2011.06.027
455
456 CAA. 2012. CAP 722 Unmanned aircraft system operations in UK airspace -
457 guidance (5th Edition). The Stationery Office, Norwich. pp 110.
458
459 Carrivick J.L., Geilhausen, M., Warburton, J., Dickson, N.E., Carver, S.J., Evans,
460 A.J. and Brown, L.E. 2012. Contemporary geomorphological activity throughout the
461 proglacial area of an alpine catchment. *Geomorphology.* **188**, 83-95.
462 http://dx.doi.org/10.1016/j.geomorph.2012.03.029
463
464 Carrivick, J.L., Smith, M.W., Quincey, D.J. and Carver, S.J. 2013. Developments in
465 budget remote sensing for the geosciences. *Geology* Today, **29** (4), 138-143.
466 http://dx.doi.org/10.1111/gto.12015
467
468 Dandois, J.P. and Ellis, E.C. 2013. High spatial resolution three-dimensional
469 mapping of vegetation spectral dynamics using computer vision. *Remote Sensing of*
470 *Environment*. **136**, 259-276. http://dx.doi.org/10.1016/j.rse.2013.04.005
471

472 Darwin, C. 1842. Notes on the effects produced by the ancient glaciers of
473 Caernavonshire, and on boulders transported by floating ice. *Philosophical*
474 *Magazine*, **3**, 180-188.
475
476 Dewitte, O., Jasselette, J.-C., Cornet, Y., Van Den Eeckhaut, M., Collignon, A.,
477 Poesen, J. and Demoulin, A. 2008. Tracking landslide displacements by multi-
478 temporal DTMs: A combined aerial stereophotogrammetric and LIDAR approach in
479 western Belgium. *Engineering Geology*. **99** (1-2), 11-22.
480
481 DJI. 2013. WooKong-M Waypoint-Altitude Offset Setting. Retrieved: 23/02/2014.
482 http://wiki.dji.com/en/index.php/WooKong-M_Waypoint-Altitude_Offset_Setting
483
484 Escritt, E.A. 1971. Plumbing the depths of Idwal's moraines. *Geographical*
485 *Magazine*, **44**, 52-55.
486
487 Fonstad, M.A., Dietrich, J.T., Courville, B.C., Jensen, J.L., Carbonneau, P.E. 2013.
488 Topographic structure from motion: a new development in photogrammetric
489 measurement. *Earth Surface Processes and Landforms*, **38**, 421-430.
490 http://dx.doi.org/10.1002/esp.3366
491
492 Fisher, P.F. and Tate, N.J. 2006. Causes and consequences of error in digital
493 elevation models. *Progress in Physical Geography*. **30** (4), 467-489.
494 http://dx.doi.org/10.1191/0309133306pp492ra
495

Graham, D.J. and Midgley, N.G. 2000. Moraine-mound formation by englacial thrusting: the Younger Dryas moraines of Cwm Idwal, North Wales. In: A.J. Maltman, B. Hubbard and M.J. Hambrey (eds.), Deformation of Glacial Materials. London: Geological Society, pp. 321-336. http://dx.doi.org/10.1144/GSL.SP.2000.176.01.24

Gray, J.M. 1982. The last glaciers (Loch Lomond Advance) in Snowdonia, North Wales. *Geological Journal*, **17**, 111-133. http://dx.doi.org/10.1002/gj.3350170204

Harwin, S. and Lucieer, A. 2012. Assessing the Accuracy of Georeferenced Point Clouds Produced via Multi-View Stereopsis from Unmanned Aerial Vehicle (UAV) Imagery. *Remote Sensing*, **4**, 1573-1599. http://dx.doi.org/10.3390/rs4061573

Hladik, C. and Alber, M. 2012. Accuracy assessment and correction of a LIDAR-derived salt marsh digital elevation model. *Remote Sensing of Environment*. **121**, 224-235. http://dx.doi.org/10.1016/j.rse.2012.01.018

Hubbard, B. and Glasser, N. 2005. Field techniques in glaciology and glacial geomorphology. New York, John Wiley & Sons.

Hugenholtz, C.H. 2010. Topographic changes of a supply-limited inland parabolic sand dune during the incipient phase of stabilization. *Earth Surface Processes and Landforms*. **35**, (14), 1674-1681. http://dx.doi.org/10.1002/esp.2053

Hugenholtz, C.H., Whitehead, K., Brown, O.W., Barchyn, T.E., Moorman, B.J., LeClair, A., Riddell, K., Hamilton, T. 2013. Geomorphological mapping with a small unmanned aircraft system (sUAS): Feature detection and accuracy assessment of a photogrammetrically-derived digital terrain model, *Geomorphology*, **194**, 16-24. http://dx.doi.org/10.1016/j.geomorph.2013.03.023

Irvine-Fynn, T.D.L,. Barrand, N.E., Porter, P.R., Hodson, A.J., and Murray, T. 2011. Recent High-Arctic proglacial sediment redistribution: a process perspective using airborne lidar. *Geomorphology*, **125**, 27-39. http://dx.doi.org/10.1016/j.geomorph.2010.08.012

James, M.R and Robson, S. 2012. Straightforward reconstruction of 3D surfaces and topography with a camera: Accuracy and geoscience application. *Journal of geophysical Research*. **117:** F03017. http://dx.doi.org/10.1029/2011JF002289

Javernick, L., Brasington, J. and Caruso, B. 2014. Modelling the topography of shallow braided rivers using Structure-from-Motion photogrammetry. *Geomorphology*. In press. Corrected Proof. http://dx.doi.org/10.1016/j.geomorph.2014.01.006

539 Jones, A.F., Brewer, P.A., Johnstone, E. and Macklin, M.G. 2007. High-resolution
540 interpretative geomorphological mapping of river valley environments using airborne
541 LiDAR data. *Earth Surface Processes and Landforms*. **32** (10): 1574-1592.
542 http://dx.doi.org/10.1002/esp.1505

543

544 Knight, J., Mitchell, W.A. and Rose, J. 2011. Geomorphological field mapping. In:
545 Smith, M.J., Paron, P. and Griffiths, J. (eds) Geomorphological Mapping: a handbook
546 of techniques and applications, Elsevier, London, 151-187.

547

548 Lane, S.N. 2000. The measurement of river channel morphology using digital
549 photogrammetry. *Photogrammetric Record*. **16** (96), 937-961.
550 http://dx.doi.org/10.1111/0031-868X.00159

551

552 Laliberte, A.S. and Rango, A. 2009. Texture and Scale in Object-Based Analysis of
553 Subdecimeter Resolution Unmanned Aerial Vehicle (UAV) Imagery. *IEEE*
554 *Transactions on Geoscience and Remote Sensing*, **47** (3), 761-770.
555 http://dx.doi.org/10.1109/TGRS.2008.2009355

556

557 Leica. 1997. TC600/800 Electronic Total Station User Manual. Lecia Geosystems,
558 Heerbrugg. 135pp.

559

560 Lucieer, A., de Jong, S.M, and Turner, D. 2013. Mapping landslide displacements
561 using Structure from Motion (SfM) and image correlation of multi-temporal UAV
562 photography. *Progress in Physical Geography*. **38** (1), 97-116.
563 http://dx.doi.org/10.1177/0309133313515293

564

565 Lucieer, A., Turner, D., King, D.H. and Robinson, S.A. 2014. Using an Unmanned
566 Aerial Vehicle (UAV) to capture micro-topography of Antarctic moss beds.
567 *International Journal of Applied Earth Observation and Geoinformation*, **27A**, 53-62.
568 http://dx.doi.org/10.1016/j.jag.2013.05.011

569

570 Lui, X. 2008. Airborne LiDAR for DEM generation: some critical issues. *Progress in*
571 *Physical Geography*. **32** (1), 31-49. http://dx.doi.org/10.1177/0309133308089496

572

573 Mancini. F., Dubbini, M., Gattelli, M., Stecchi, F., Fabbri, S. and Gabbianelli, G.
574 2013. Using Unmanned Aerial Vehicles (UAV) for High-Resolution Reconstruction of
575 Topography: The Structure from Motion Approach on Coastal Environments. *Remote*
576 *Sensing*, **5**, 6880-6898. http://dx.doi.org/10.3390/rs5126880

577

578 Marzolff, I. and Poesen, J. 2009. The potential of 3D gully monitoring with GIS using
579 high-resolution aerial photography and a digital photogrammetry system.
580 *Geomorphology*, **111** (1-2), 48-60. http://dx.doi.org/10.1016/j.geomorph.2008.05.047

581

582 Mitasova, H., Overton, M.F., Recalde, J.J., Bernstein, D.J and Freeman, C.W. 2009.
583 Raster-Based Analysis of Coastal Terrain Dynamics from Multitemporal Lidar Data.
584 *Journal of Coastal Research*. **25** (2), 507-514. http://dx.doi.org/10.2112/07-0976.1

585

586 Niethammer, U., James, M.R., Rothmund, S., Travelletti, J. and Joswig, M. 2012.
587 UAV-based remote sensing of the Super-Sauze landslide: Evaluation and results.
588 *Engineering Geology*, **128**, 2-11. http://dx.doi.org/10.1016/j.enggeo.2011.03.012

589

590 Oguchi, T., Hayakawa, Y.S. and Wasklewicz, T. 2011. Data Sources. In: Smith, M.J.,
591 Paron, P. and Griffiths, J. (eds) Geomorphological Mapping: a handbook of
592 techniques and applications, Elsevier, London, 151-187.

593

594 Ouédraogo, M.M., Degré, A., Debouche, C. and Lisein, J. 2014. The evaluation of
595 unmanned aerial system-based photogrammetry and terrestrial laser scanning to
596 generate DEMs of agricultural watersheds. *Geomorphology*, **214**, 339–355.
597 http://dx.doi.org/10.1016/j.geomorph.2014.02.016

598

599 Pyle, C.J., Richards, K.S. and Chandler, J.H. 1997. Digital photogrammetric
600 monitoring of river bank erosion. *The Photogrammetric Record*. **15**, 753–764.
601 http://dx.doi.org/10.1111/0031-868X.00083

602

603 Rango, A., Laliberte, A., Herrick, J.E., Winters, C., Havstad, K., Steele, C. and
604 Browning, D. 2009. Unmanned aerial vehicle-based remote sensing for rangeland
605 assessment, monitoring and management. *Journal of Applied Remote Sensing*: **3**, 1-
606 15. http://dx.doi.org/10.1117/1.3216822

607

608 Rosnell, T and Honkavaara, E. 2012. Point Cloud Generation from Aerial Image
609 Data Acquired by a Quadrocopter Type Micro Unmanned Aerial Vehicle and Digital
610 Still Camera. *Sensors*, **12**, 453-480. http://dx.doi.org/10.3390/s120100453

611

612 Rhind, P. and Jones, B. The vegetation history of Snowdonia since the Last Glacial
613 Period. *Field Studies*, **10**, 539-552.

614

615 Schiefer, E. and Gilbert, R. 2007. Reconstructing morphometric change in a
616 proglacial landscape using historical aerial photography and automated DEM
617 generation. **88** (1-2), 167-178. http://dx.doi.org/10.1016/j.geomorph.2006.11.003

618

619 Smith, M.J., Chandler, J. and Rose, J. 2009. High spatial resolution data acquisition
620 for the geosciences: kite aerial photography. *Earth Surface Processes and*
621 *Landforms*. **34**, 155-161. http://dx.doi.org/10.1002/esp.1702

622

623 Snavely, N., Seitz, S.M. and Szeliski, R. 2008. Modelling the World from Internet
624 Photo Collections. *International Journal of Computer Vision*. **80** (2), 189-210.
625 http://dx.doi.org/10.1007/s11263-007-0107-3

626

627 Spaete, L.P., Glenn, N.F., Derryberry, D.R., Sankey, T.T., Mitchell, J.J., and
628 Hardegree, S.P. 2011. Vegetation and slope effects on accuracy of a LiDAR-derived
629 DEM in the sagebrush steppe. *Remote Sensing Letters*, **2** (4), 317-326.
630 http://dx.doi.org/10.1080/01431161.2010.515267

631

632 Tarolli, P. 2014. High-resolution topography for understanding Earth surface
633 processes: opportunities and challenges. *Geomorphology*, **216**, 295-312.
634 http://dx.doi.org/10.1016/j.geomorph.2014.03.008

635

636 Turner, D., Lucieer, A. and Watson, C. 2012. An Automated Technique for
637 Generating Georectified Mosaics from Ultra-High Resolution Unmanned Aerial
638 Vehicle (UAV) Imagery, Based on Structure from Motion (SfM) Point Clouds. *Remote*
639 *Sensing*, **4**, 1392-1410. http://dx.doi.org/10.3390/rs4051392

640

641 Wechsler, S.P. 2007. Uncertainties associated with digital elevation models for
642 hydrologic applications: a review. *Hydrology and Earth System Sciences*, **11**, 1481-
643 1500. http://dx.doi.org/10.5194/hess-11-1481-2007

644

645 Westoby, M.J., Brasington, J., Glasser, N.F., Hambrey, M.J., and Reynolds, J.M.
646 2012. 'Structure-from-motion' photogrammetry: A low-cost, effective tool for
647 geoscience applications. *Geomorphology*: **179**, 300-314.
648 http://dx.doi.org/10.1016/j.geomorph.2012.08.021

649

650 Wester-Ebbinghaus, W. 1980. Aerial Photography by radio controlled model
651 helicopter. London. England. *The Photogrammetric Record*. Vol. X No. 55.
652 http://dx.doi.org/10.1111/j.1477-9730.1980.tb00006.x

653

654 Whitehead, K., Moorman, B.J. and Hugenholtz, C.H. 2013. Brief Communication:
655 Low-cost, on-demand aerial photogrammetry for glaciological measurement. *The*
656 *Cryosphere*, **7**, 1879-1884. http://dx.doi.org/10.5194/tc-7-1879-2013

657

658 Williams, R.D. 2012. Section 2.3.2: DEMs of difference (using DODs to quantify
659 landscape change and uncertainty analysis in DoDs). In: Clarke, L.E & Nield, J.M.
660 (Eds.) Geomorphological Techniques (Online Edition). British Society for
661 Geomorphology; London, UK. ISSN: 2047-0371.

Fig. 1 Maps showing the study site location in relation to (a) North-west Europe, and (b) North Wales. ©Crown Copyright/database right 2014. An Ordnance Survey/EDINA supplied service. (c) A ground-level panoramic photograph of the moraine-mound complex which is located on both the left and right of Llyn Idwal.

Fig. 2 A schematic drawing of the S800 hexacopter.

Fig. 3 Maps displaying the topographic data and analysis of vertical disagreement. (a) The distribution of 7761 ground-survey points and 19 SfM ground-control points across the survey area. Two zones (Z1 and Z2) of distinct ground cover are delimited. (b) A hillshaded DSM at 0.088 m per pixel resolution derived from the sUAS–SfM survey. (c) A raster surface of vertical difference produced using an ordinary kriging function at a resolution of 2.1 m per pixel. The spatial extent of the spot heights is delimited by the dashed line.

Fig. 5 The occurrence of vertical difference in association with: (a) vegetation, (b) near vertical and in places partially overhanging bedrock rafts, and (c) positional misregistration close to near vertical slopes

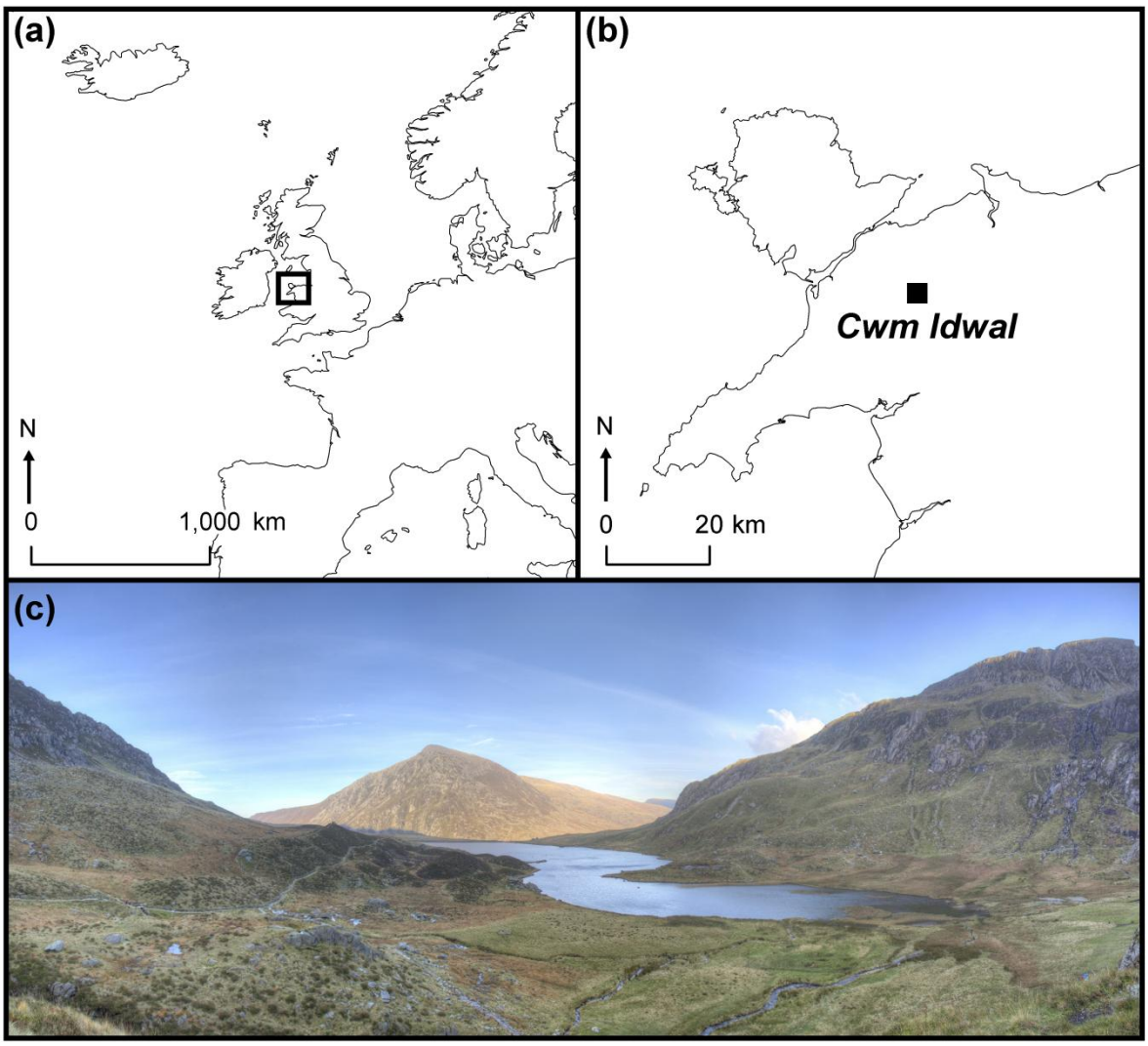

681

682

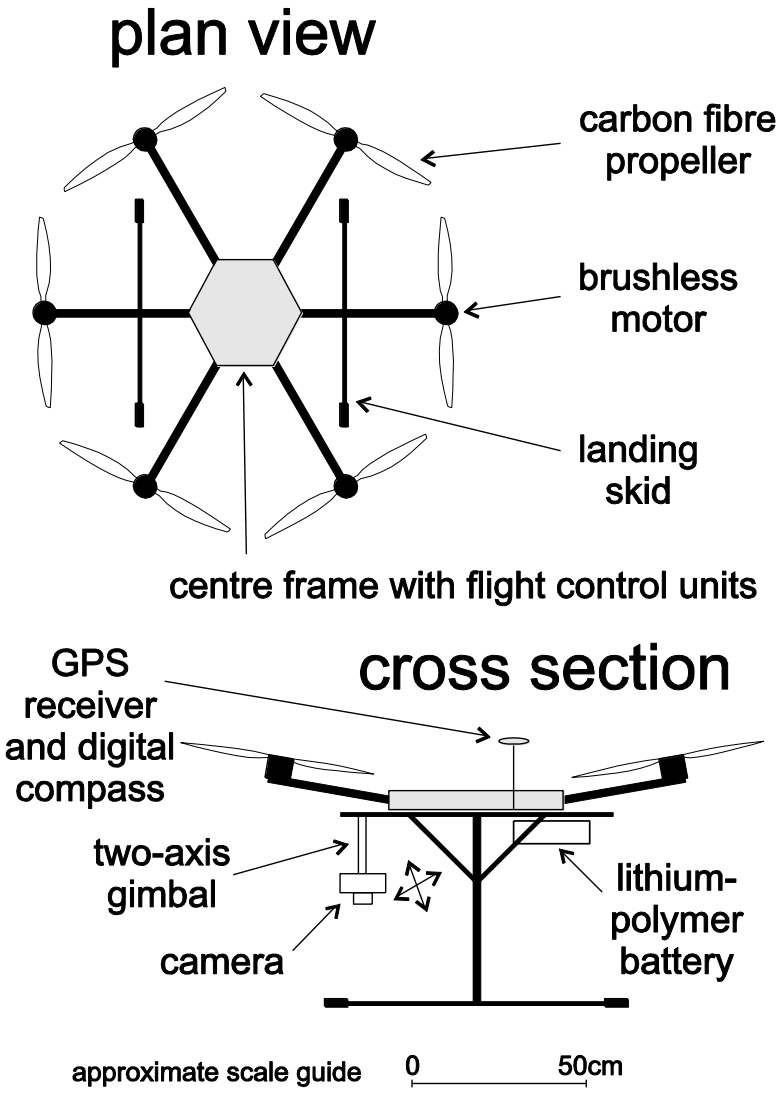
plan view
carbon fibre propeller
brushless motor
landing skid
centre frame with flight control units
cross section
GPS receiver and digital compass
two-axis gimbal
camera
lithium-polymer battery
approximate scale guide
0
50cm

683

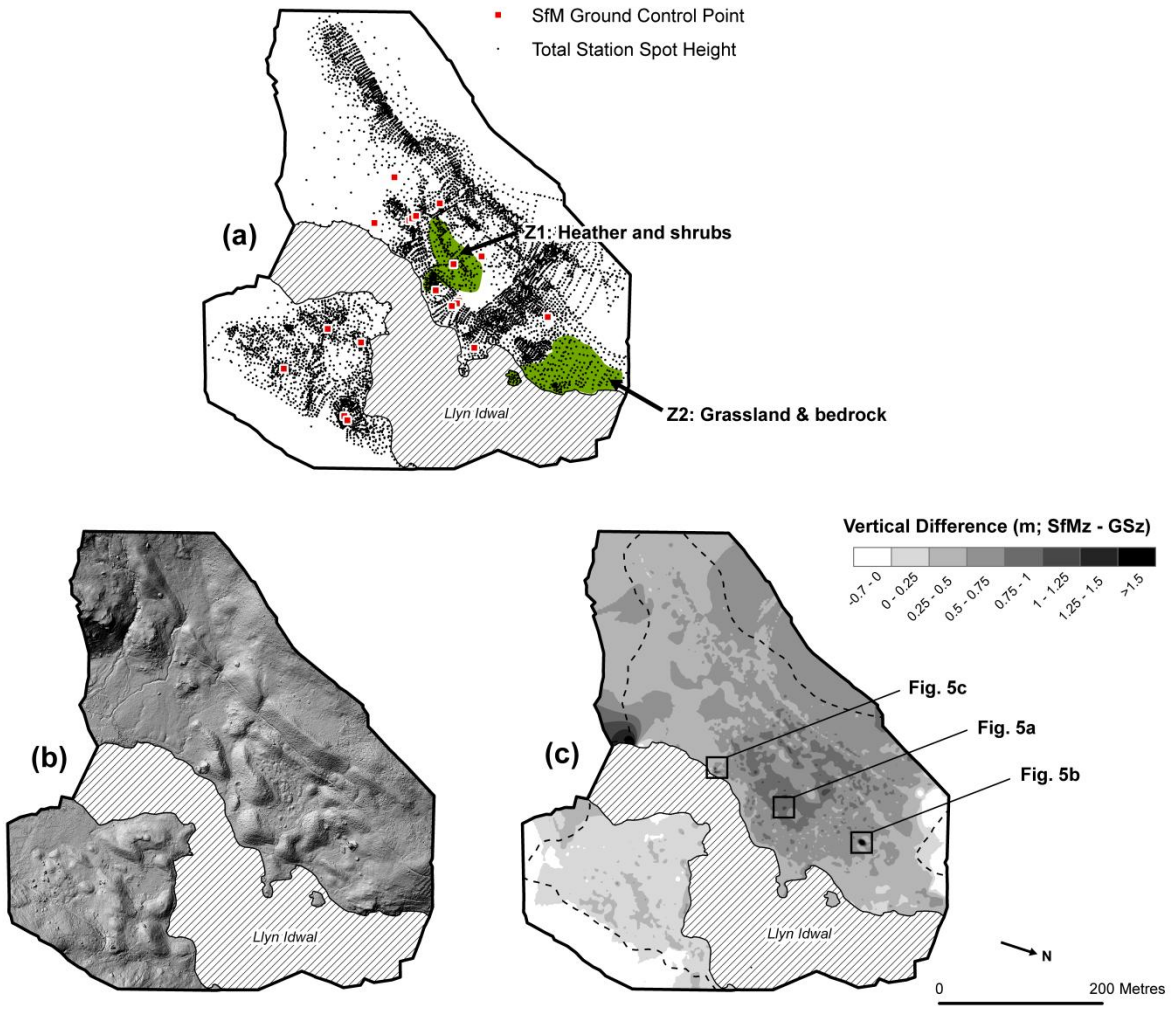
SfM Ground Control Point
Total Station Spot Height
(a)
Z1: Heather and shrubs
Z2: Grassland & bedrock
Llyn Idwal
(b)
Llyn Idwal
Vertical Difference (m; SfMz - GSz)
-0.7 - 0
0 - 0.25
0.25 - 0.5
0.5 - 0.75
0.75 - 1
1 - 1.25
1.25 - 1.5
>1.5
(c)
Fig. 5c
Fig. 5a
Fig. 5b
Llyn Idwal
N
0
200 Metres

684

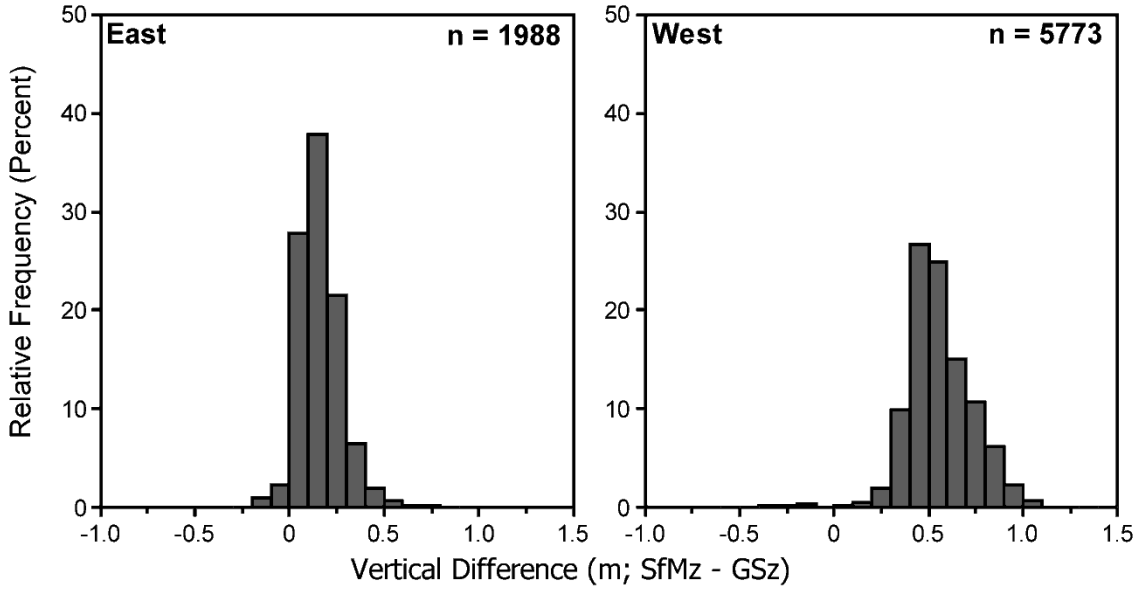
East
n = 1988
West
n = 5773
Relative Frequency (Percent)
Vertical Difference (m; SfMz - GSz)
0
10
20
30
40
50
-1.0
-0.5
0
0.5
1.0
1.5

685

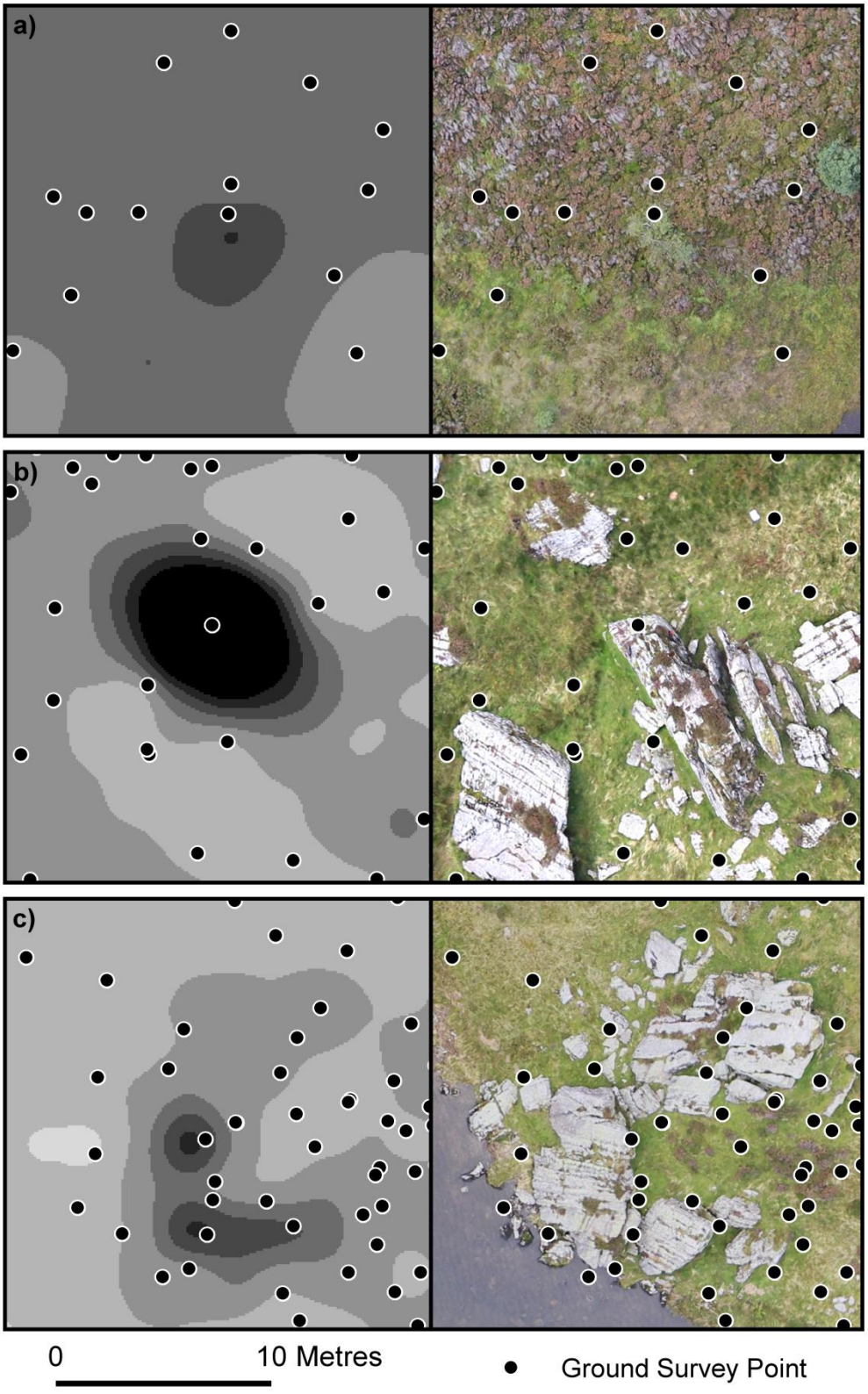
a)
b)
c)
0
10 Metres
Ground Survey Point
Vertical Difference (m; SfMz - GSz)
-0.7 - 0
0 - 0.25
0.25 - 0.5
0.5 - 0.75
0.75 - 1
1 - 1.25
1.25 - 1.5
>1.5

686

687 **Table 1** Statistics for the vertical difference between the Cwm Idwal topographic

688 datasets

Area	*Total Observations (n)*	*RMSE*	*MD* [a]	*RMSE (<20°)*	*RMSE (≥20°)*
All	7761	0.517	0.454	0.468 (*n* = 4527)	0.578 (*n* = 3234)
East	1988	0.200	0.155	0.169 (*n* = 1306)	0.247 (*n* = 682)
West	5773	0.588	0.557	0.544 (*n* = 3222)	0.639 (*n* = 2551)
Z1	244	0.796	0.820	0.789 (*n* = 102)	0.821 (*n* = 142)
Z2	205	0.362	0.341	0.354 (*n* = 152)	0.384 (*n* = 53)

689 [a] *Mean Difference*

690 **Table 2** Calculated RMSE for vertical difference binned by slope angle.

Bin	*RMSE*	*Observations (n)*
0 – 9	0.444	1864
10 – 19	0.482	2662
20 – 29	0.543	1967
30 – 39	0.603	952
40 – 49	0.678	263
50 – 59	0.739	36
60 – 69	0.729	10
70 – 79	0.838	6
80 – 90	2.222	1

691

692

693 **Table 3** Comparative table of known vertical differences between SfM topographic
694 surveys and various validation datasets in a range of geomorphological
695 environments

Study	*Geomorphological setting*	*Camera*	*Camera Platform*	*Survey Altitude (m AGL)*	*Validation Data*	*Vertical Difference*
Westoby et al. (2012)	Coastal	SLR: Model not specified	None	Ground-level	Terrestrial Laser Scanner	94% points values within +/- 1 m
Hugenholtz et al.. (2013)	Aeolian	Olympus PEN Mini E-PM1	Fixed-wing sUAS	200	RTK GPS	RMSE = 0.29 m
Fonstad et al. (2013)	Exposed Bedrock/Fluvial	Canon A480	Helikite	10-70	LiDAR	RMSE = 1.05 m
Javernick et al.. (2014)	Fluvial (Braided Channel)	Canon (10.1 MP): Model not specified.	Full-scale helicopter	600-800	RTK GPS	RMSE = 0.13 – 0.37 m
This study	Glacial landforms (Vegetated)	Canon EOS-M (18 MP)	Multi-rotor sUAS	117 (average)	Total Station	RMSE = East: 0.200 m West: 0.588 m All: 0.517 m

696